Martin Sobczyk, Thomas Wallmersperger

Modeling and simulation of the electro-chemical behavior of chemically stimulated polyelectrolyte hydrogel layer composites

Erstveröffentlichung in / First published in:

Journal of Intelligent Material Systems and Structures. 2016, 27(13), S. 1725 - 1737 *[Zugriff am: 12.08.2019]*. SAGE journals. ISSN 1530-8138.

DOI: https://doi.org/10.1177/1045389X15606997

Journal of
Intelligent Material
Systems and Structures

Original Article

Journal of Intelligent Material Systems and Structures
2016, Vol. 27(13) 1725–1737

DOI: 10.1177/1045389X15606997
jim.sagepub.com
SAGE

Modeling and simulation of the electro-chemical behavior of chemically stimulated polyelectrolyte hydrogel layer composites

Martin Sobczyk and Thomas Wallmersperger

Abstract

Polyelectrolyte hydrogels are viscoelastic electroactive polymers which respond to external physical or chemical stimuli by a reversible volume phase transition. Novel fabrication methods allow the creation of hydrogel layer composites in which each layer shows a different sensitivity (e.g. to a different stimulus). This offers new opportunities, for example, in the design of new microsensors, microactuators and microfluidic devices as well as for high-selective membranes and target-specific drug delivery systems. Since only few research groups numerically investigated the transport mechanisms in hydrogel layer composites, a gap remains to describe the movement and transient distribution of ions inside the layer system.

In this article, the multifield formulation is adopted to describe the transient distribution of ions in salt-sensitive hydrogel layer composites on the basis of a numerical simulation. For this, the Nernst-Planck and the Poisson equation are solved using one-dimensional finite elements for both anionic-anionic and anionic-cationic gel layer composites under chemical stimulation. Between adjacent gels, an additional interlayer is introduced to account for the physical and chemical bonding region between the gels. Adaptive mesh refinement provides a good resolution close to the interface between the adjacent gel layers. The obtained results are used to predict the osmotic pressure inside the gels and the dependent swelling of the gel layer composite. The excellent agreement of the obtained results with the Donnan equilibrium demonstrates the high potential of the method applied to predict the behavior of hydrogel layer composites.

Keywords

Hydrogel, layer composites, thin layers, multifield theory, modeling, transient behavior, interlayer, finite element method

Introduction

The International Union of Pure and Applied Chemistry (IUPAC) defines a gel as a nonfluid, colloidal or polymer network which is filled with a liquid (Slomkowski et al., 2011). Typically, gels exhibit a small yield stress. They may contain:

- a covalent polymer network;
- a polymer network formed through the physical aggregation of polymer chains (caused by hydrogen bonds, crystallization, helix formation, complexation, etc.);
- a polymer network formed through glassy junction points, for example, a polymer network based on block copolymers;
- lamellar structures including mesophases, for example, soap gels, phospholipids, and clays;
- particulate disordered structures, for example, a flocculent precipitate.

Hydrogels with a colloidal network component, which swell in water can be referred to as aquagels. Gels comprising a polymeric network component are called polymeric hydrogels. If a polymeric hydrogel contains a considerable portion of ionizable groups, it is called a polyelectrolyte gel.

The present article focuses on the chemo-electrical behavior of polyelectrolyte gel layer composites. In the following, polyelectrolyte gels will be referred to as hydrogels.

For a hydrogel $\mathcal{G}$ to have sensing or swelling capabilities, it has to be immersed in an ionic solution bath $\mathcal{S}$,

Institut für Festkörpermechanik, Technische Universität Dresden, Germany

Corresponding author:
Thomas Wallmersperger, Institut für Festkörpermechanik, Technische Universität Dresden, 01062 Dresden, Germany.
Email: thomas.wallmersperger@tu-dresden.de

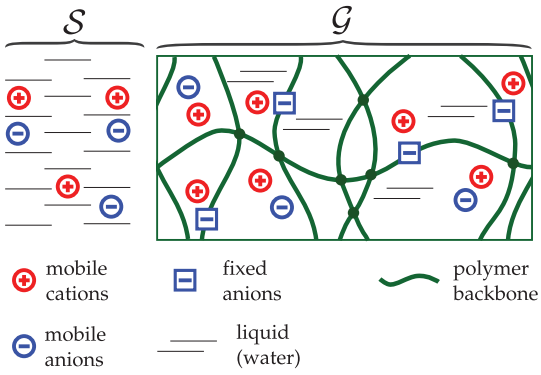

Figure 1. Schematic representation of a hydrogel structure $\mathcal{G}$, immersed in an ionic solution bath $\mathcal{S}$. The polymer chains can be regarded as neutral polymer backbone with bound (fixed) ionic groups. Within the gel and the solution, water and mobile ions are present.

containing mobile anions and cations, see Figure 1. A hydrogel $\mathcal{G}$ can be regarded as a hydrophobic polymer backbone with ionic, and therefore hydrophilic, functional groups. The ions in the solution bath are able to move freely through the hydrogel due to diffusion, migration and convection processes. The ionic functional groups of the polymer backbone are treated as fixed ions, since they can only move in connection to the polymer network.

Hydrogels have gained a lot of attention due to their ability to swell in response to physical, chemical or biochemical stimuli (Jeong and Gutowaka, 2002; Osada and Gong, 1998; Qiu and Park, 2001; Wu et al., 2004).

Recent advances in nanotechnology led to an increased interest in hydrogel thin films. They can be manufactured with different techniques, for example, by crosslinking copolymerization (adding multifunctional comonomers), crosslinking (co)polymers with reactive groups and crosslinking with high-energy irradiation (Tokarev and Minko, 2009). Physically crosslinked films were prepared by polyelectrolyte complexation (e.g. layer-by-layer assembly) (Hiller and Rubner, 2003; Kharlampieva et al., 2005) and block-copolymer self-assembly (Nykänen et al., 2007). For the crosslinking copolymerization, solvent-based free-radical polymerization is often adopted (Harmon et al., 2002), where the monomers, a crosslinking agent and a free-radical initiator are spin coated or polymerized between two planar surfaces. The crosslinking via reactive groups is usually started by activation of reactive groups by thermal heating or radiation exposure (Kuckling et al., 2002; Richter et al., 2004; Tokarev and Minko, 2009). High-energy irradiation is a crosslinking agent free technique, where an electron beam, gamma-ray or UV-radiation is utilized to randomly open up chemical bonds and let the generated radicals recombine to form new bonds (Tokarev and Minko, 2009).

For some applications, hydrogels that exhibit a swelling behavior in response to more than one stimulus are needed. Hydrogels or systems composed of different hydrogels, which respond to two or multiple stimuli are referred to as bi- or multi-sensitive hydrogels, respectively.

A possible way to fabricate bisensitive hydrogel layer composites is to stack and fuse a number of hydrogel thin layers. For this, Fulghum et al. (2008) synthesized a composite hydrogel layer with a pH-sensitive and a temperature-sensitive layer by combining layer-by-layer and surface-initiated polymerization techniques. They used the weak polyelectrolytes poly(allylamine hydrochloride) (PAH) and poly(acrylic acid) (PAA) to create the pH-sensitive layer, capable of surface-initiated polymerization. On top of this layer, n-isopropylacrylamide was polymerized to form thermo-responsive poly(n-isopropylacrylamide) (PNIPAAm) brushes. Jaber and Schlenoff (2005) were able to demonstrate thermally reversible ion transport modulation by forming thermally responsive polyelectrolyte multilayers from charged PNIPAAm copolymers. With this approach, a layer-by-layer sequential assembly from ionically modified PNIPAAm copolymers was realized. Further works on the construction of multi-responsive hydrogel layers were published (Nolan et al., 2004; Serpe et al., 2005).

The layer composite design offers the possibility to create superior drug carriers for medical treatment or for novel high-selective membranes. In order to fulfill the high requirements of the membrane industry and the medical sector, a profound knowledge of the hydrogel material behavior is necessary. The osmotic pressure and the resulting swelling of the hydrogel directly depend on the ion concentrations in the gel and the surrounding solution. Therefore it is of great interest to investigate the coupled chemo-electrical behavior of the hydrogel system.

Hydrogel layer systems are highly interesting for possible applications, but their behavior remains challenging to describe. Since only few research groups (Lu et al., 1998, 2000; Lucantonio et al., 2014; Sohier et al., 2006) modeled the behavior of hydrogel layer systems, a gap in understanding the coupled phenomena occurring within the gel networks remains. The present article contributes to fill this gap by modeling the electrochemical behavior of two chemically different hydrogel layer composites. First, a chemically stimulated anionic-anionic hydrogel layer composite will be investigated and the obtained results for the ion distribution, the electric potential and the volume charge density will be discussed. Then an anionic-cationic gel layer composite is modeled to compare the results with the first test case. In both hydrogel layer systems, an additional gel layer that is responsible for mechanical stability is considered. The investigated system is depicted schematically in Figure 2. The chemo-electrical multifield theory

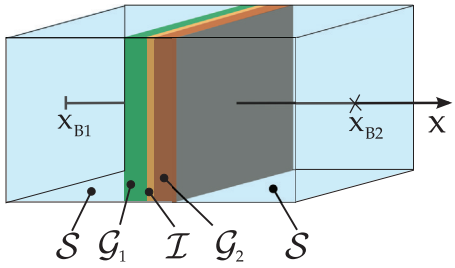

Figure 2. Schematic representation of the investigated hydrogel layer system. It is composed of two hydrogels $\mathcal{G}_1$ and $\mathcal{G}_2$ with a connecting interlayer $\mathcal{I}$. The composite is immersed in a solution bath $\mathcal{S}$, delimited at the boundaries x_{B1} and x_{B2} in 1D.

is adopted and applied on the different hydrogel layer composites. By this approach, the diffusion, migration and convection of particles through the gel system can be investigated. Since hydrogel layer systems comprise more than one gel domain, the interface and the occurring transport phenomena between neighboring domains are of particular interest.

Modeling approaches in the literature

As early as in the 1940s, Flory and Rehner (1943a,b) were the first to describe the equilibrium swelling of a polymer network (rubber) by formulating a macroscopic theory. One of the first groups to describe transient phenomena by coupling effects in hydrogels were Grimshaw et al. (1990), Shiga and Kurauchi (1990), Doi et al. (1992), and Shahinpoor (1995). At about the same time Brock et al. (1994) described the design and analysis of a series of linear actuators based on hydrogels using a dynamic model. Huyghe and Janssen (1997) and Lai et al. (1991) were some of the first to describe the quasi-static finite deformation due to the swelling of a hydrogel using the theory of porous media (Bowen, 1980).

A finite element model describing the behavior of soft tissue constituents (charged solid, fluid, two mobile charged species) was given by Sun et al. (1999) and van Loon et al. (2003). In the work of de Gennes et al. (2000), mechano-electrical effects ((i) mechanical deformation due to an applied voltage, (ii) electric current due to mechanical deformation) in hydrogels were modeled. To investigate the effects of an electrical or chemical stimulation on a hydrogel, Wallmersperger et al. (2001, 2004) used an electro-chemical and electro-chemo-mechanical formulation. A further multiphysical approach for the simulation on pH-sensitive hydrogels was pursued by De et al. (2002) to describe its chemo-electro-mechanical behavior. Based on the theory of porous media, Ehlers et al. (2003a,b) and Acartürk et al. (2003) described the swelling of pH-sensitive hydrogels. Li et al. (2007) solved a chemo-electro-mechanical field problem describing the hydrogel behavior using a hermite meshless discretization method (Li et al., 2003). Employing molecular dynamics simulations of a coarse-grained model, Mann et al. (2005, 2006) investigated the equilibrium swelling of a bead-spring defect-free polymer network. A characterization of hydrogel based sensor devices was done by Gerlach et al. (2005), Richter et al. (2004) and Guenther et al. (2009).

Orlov et al. (2006, 2007), Ermatchkov et al. (2010), Prudnikova and Utz (2012) and Arndt and Sadowski (2013) performed equilibrium swelling experiments with hydrogels and compared the results with thermodynamic based models. The temperature dependence of swelling of PNIPAAm hydrogels in pure water was studied both experimentally and by molecular simulation by Walter et al. (2010). Keller et al. (2011) described the swelling behavior of temperature-sensitive hydrogels for gels with decreasing and increasing swelling ratio with rising temperatures using an additional temperature-dependent osmotic pressure term.

A numerical investigation of hydrogel layer systems was conducted by Lu et al. (1998, 2000) and Sohier et al. (2006), describing the drug release profiles using a model based on Fick's law. Recently, Lucantonio et al. (2014) modeled the chemo-electro-mechanical behavior of hydrogel bars under the assumption that the occurring large bending deformation can be multiplicatively split into the uniform free-swelling stretch and a further elastic contribution.

A specific investigation on the ion distribution and the occurring electric field within hydrogel layer composites is necessary, but has not been conducted yet.

Chemo-electrical field formulation

In the following, the coupled chemo-electrical field problem for the investigation of hydrogel layer systems is reviewed. In this model, the hydrogel and the surrounding solution are treated as a triphasic continuum including a solid polymer backbone with bound ionic groups and two mobile ion species (e.g. Cl^- and Na^+). The chemo-electrical field formulation is given in the tradition of other research groups (Ballhause and Wallmersperger, 2008; De et al., 2002; Doi et al., 1992; Johnson and Amirouche, 2008; Lucantonio et al., 2014; Shahinpoor, 1995; Wallmersperger et al., 2001, 2004) who work in this field. In the following, a coupled chemo-electrical field formulation for a composite hydrogel layer system is given. For further insight into the derivation of the applied equations, the reader is referred to Attaran et al. (2015).

Chemical field formulation

The chemical field describing the temporal and spatial distribution of mobile charged species in a domain can be evaluated by solving the diffusion-migration-convection partial differential equation

$$\dot{c}_\alpha = \underbrace{[D_\alpha c_{\alpha,i}}_{\text{diffusion}} + \underbrace{D_\alpha \frac{F}{RT} z_\alpha c_\alpha \Psi_{,i}]_{,i}}_{\text{migration}} \underbrace{-(c_\alpha v_i)_{,i}}_{\text{convection}} + \underbrace{r_\alpha}_{\text{source term}} \tag{1}$$

Here, the temporal change of the chemical concentration c_α of the species α is calculated from the sum of a diffusive, a migrative and a convective term as well as a contribution by sources and sinks due to chemical conversion. The variable D_α denotes the diffusion constant of the species α, z_α its valence (charge number), F the Faraday constant, R the universal gas constant, T the absolute temperature in Kelvin, Ψ the electric potential, v the velocity of the fluid and r_α a source term resulting from chemical reactions involving the species α. The index $i \in [1, 2, 3]$ describes the spatial direction x_i. The operators $\dot{()}$ and $()_{,i}$ denote the time derivative $\frac{\partial}{\partial t}$ and the spatial derivative $\frac{\partial}{\partial x_i}$, respectively. Equation (1) is obtained from the conservation of mass

$$\dot{c}_\alpha = -J^\alpha_{i,i} + r_\alpha \tag{2}$$

The flux J^α_i of the species α into and out of a reference volume can be expressed as the sum of a diffusive flux, resulting from concentration differences, a migrative flux, stemming from a gradient of the electric potential and a convective flux due to the velocity of the solvent

$$J^\alpha_i = -D_\alpha c_{\alpha,i} - D_\alpha \frac{F}{RT} z_\alpha c_\alpha \Psi_{,i} + c_\alpha v_i \tag{3}$$

Here, the dissociation reaction of water is neglected, since the concentration of hydronium and hydroxide ions is assumed to be small compared to c_α.

Electrical field formulation

The electrical field formulation can be obtained by using Gauss' law

$$\tilde{D}_{i,i} = \rho_{el} \tag{4}$$

where $\tilde{D}$ and ρ_{el} are the electric displacement and the volume charge density, respectively. The volume charge density describes the charges Q per Volume V and can be expressed by

$$\rho_{el} = \frac{Q}{V} = F \sum_{\alpha=1}^{N_f + N_b} z_\alpha c_\alpha \tag{5}$$

where N_f and N_b are the number of freely movable and bound charged species, respectively. The propagation speed of the electric field is much higher than the velocity of electrically charged species. Therefore the quasi-static form of the Maxwell-Faraday equation can be adopted. It yields

$$\tilde{\varepsilon}_{ijk} E_{k,j} = -\frac{\partial B_i}{\partial t} = 0 \tag{6}$$

Here, $\tilde{\varepsilon}_{ijk}$ denotes the permutation tensor, E_i the electric field and B_i the magnetic field. Equation (6) shows that the rotation of the electric field equals zero. In this case, it is curl free and can be expressed as the gradient of the electric potential Ψ, if the domain is simply connected

$$\Psi_{,i} = -E_i \tag{7}$$

For a linear, homogeneous and isotropic dielectric material the constitutive equation linking the electric displacement $\tilde{D}_i$ and the electric field E_i reads

$$\tilde{D}_i = \varepsilon_0 \varepsilon_r E_i \tag{8}$$

Here, ε_r and ε_0 are the relative and the vacuum permittivity, respectively. With the given equations, the electrical field formulation can be written as

$$\Psi_{,ii} = -\frac{F}{\varepsilon_r \varepsilon_0} \sum_{\alpha=1}^{N_f + N_b} z_\alpha c_\alpha \tag{9}$$

Coupling of the chemical and electrical field

Equations (1) and (9) are coupled by the ion concentrations c_α and the electric potential Ψ. To solve the fully coupled nonlinear field problem, suitable boundary conditions have to be prescribed. These can be the electric potential Ψ or its associated flux, the electric displacement $\tilde{D}_i$. Additionally, boundary conditions for either the ion concentrations c_α or the ion flux J^α_i have to be prescribed at the boundaries.

Since equation (1) represents an initial boundary value problem, adequate initial conditions for the coupled field problem are required in c_α and Ψ.

Between neighboring domains transition conditions have to be formulated. Here, continuity of the primary variables (electric potential and the ion concentrations) and the fluxes (electric displacement and ion flux) is prescribed, which is naturally fulfilled by the applied finite element formulation. The different domains are distinguished by using different material parameters.

Discretization

To solve the described chemo-electrical field problem an analytical approach is feasible, as shown by Farinholt and Leo (2004) for the modeling of ionic polymer-metal composites. In order to gain more flexibility with respect to the prescribed initial and boundary conditions as well as for the possibility to extend the model to a 2D or 3D domain, the set of partial differential equations is solved by using the finite element method. As a first step, the modeling is conducted and realized one-dimensionally.

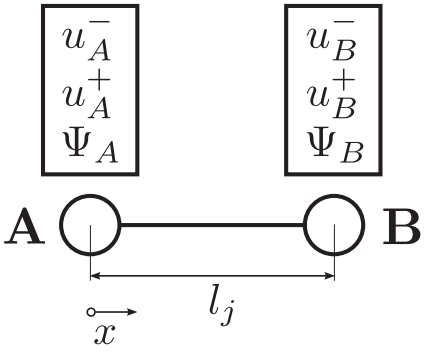

Figure 3. Two-noded element with its nodal unknowns and its element length l_j.

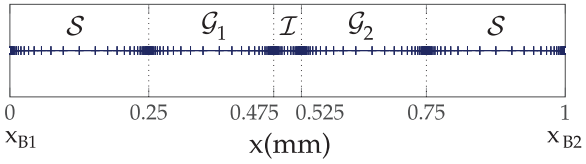

Figure 4. Adaptive mesh refinement with a high resolution at the boundaries between neighboring domains ($\mathcal{S}$,$\mathcal{G}_1$,$\mathcal{I}$,$\mathcal{G}_2$,$\mathcal{S}$).

The equations (1) and (9) are discretized in time using the implicit Euler method. The coupled nonlinear system of equations is discretized using linear shape functions for both, the weighting and the ansatz functions and linearized using the Newton method.

The domains, comprising the gel layers and a surrounding solution bath are spatially discretized using two noded linear elements. The coupling of the chemical and the electrical field can be given by the element matrices

$$\underbrace{\begin{bmatrix} \mathbf{D}_{cc} & \mathbf{0} \\ \mathbf{0} & \mathbf{0} \end{bmatrix}}_{\mathbf{D}} \underbrace{\begin{bmatrix} \Delta\dot{\mathbf{c}} \\ \Delta\dot{\Psi} \end{bmatrix}}_{\Delta\dot{\mathbf{u}}} + \underbrace{\begin{bmatrix} \mathbf{K}_{cc} & \mathbf{K}_{c\Psi} \\ \mathbf{K}_{\Psi c} & \mathbf{K}_{\Psi\Psi} \end{bmatrix}}_{\mathbf{K}} \underbrace{\begin{bmatrix} \Delta\mathbf{c} \\ \Delta\Psi \end{bmatrix}}_{\Delta\mathbf{u}} = \underbrace{\begin{bmatrix} \mathbf{R}_c \\ \mathbf{R}_\Psi \end{bmatrix}}_{\mathbf{R}_u} \tag{10}$$

Here, $\mathbf{D}$, $\mathbf{K}$, and $\mathbf{R}_u$ are the damping matrix, the stiffness matrix and the residual vector, respectively. The submatrices $\mathbf{K}_{\Psi c}$ and $\mathbf{K}_{c\Psi}$ are responsible for the coupling between the electrical and the chemical field. The vector of the increments of the nodal unknowns is defined as $\Delta\mathbf{u}^{\mathrm{T}} = [\Delta c_{\mathrm{A}}^-, \Delta c_{\mathrm{B}}^-, \Delta c_{\mathrm{A}}^+, \Delta c_{\mathrm{B}}^+, \Delta\Psi_{\mathrm{A}}, \Delta\Psi_{\mathrm{B}}]$, where the indices A and B refer to the respective node. The developed 1D finite element is displayed in Figure 3.

A mesh refinement at the interfaces between neighboring domains is accomplished via an adaptive mesh, as depicted in Figure 4. For this, each domain is discretized symmetrically, see Figure 5. The length of each element in the first half of a domain ($\mathcal{S}$,$\mathcal{G}_1$,$\mathcal{I}$, or $\mathcal{G}_2$) can be described by

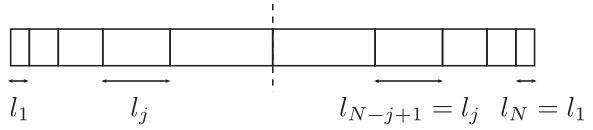

Figure 5. Mesh refinement within one domain. The element length decreases exponentially from the center towards the boundaries of the domain, yielding a high resolution at the boundary regions.

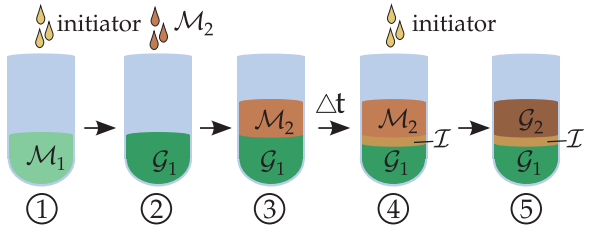

Figure 6. Fabrication steps to combine two different polymer networks. The hydrogels are synthesized from monomer solutions containing a crosslinking agent by adding an initiator.

$$l_j = l_1 \cdot g^j \tag{11}$$

where l_j and l_1 denote the length of element number j in the domain and the length of the first element in the domain, respectively. The constant g describes the ratio of an element length to its predecessor

$$g = \frac{l_j}{l_{j-1}} \tag{12}$$

Since each domain is discretized symmetrically, the length of each element in the second half of a domain can be given by

$$l_{N-j+1} = l_j \tag{13}$$

where N is the number of elements in the domain.

Realization of an interlayer between neighboring gel domains

It is assumed, that the hydrogels in the gel layer composite are synthesized from monomer solutions containing a crosslinker by adding an initiator to the monomer solutions. To yield a mechanically stable layer composite, the gels are successively synthesized on top of each other, see Figure 6. The fabrication steps are;

1. Monomer solution $\mathcal{M}_1$ containing the crosslinker is filled into a containment. The polymerization is started by addition of an initiator.
2. After gel $\mathcal{G}_1$ is formed from monomer solution $\mathcal{M}_1$, monomer solution $\mathcal{M}_2$ is added on top of the gel $\mathcal{G}_1$.

3. The monomer solution is allowed to diffuse into the polymer network of gel $\mathcal{G}_1$ for some time Δt.
4. The region $\mathcal{I}$ describes the region where particles of the monomer solution and the polymer chains of gel $\mathcal{G}_1$ coexist. The polymerization of monomer solution $\mathcal{M}_2$ is started by addition of an initiator.
5. Gel $\mathcal{G}_2$ has been formed from monomer solution $\mathcal{M}_2$. Within the interlayer region $\mathcal{I}$ the adjacent gels are physically connected.

The region in which polymer chains of the different polymer networks coexist should exhibit different material parameters than each of the gels by themselves, since it contains volume fractions of both gels. In this article this interlayer region is accounted for by modeling an additional gel layer with distinct material parameters.

Recently the described fabrication method was successfully applied to synthesize a composite of a polyelectrolyte and a non-polyelectrolyte gel, see Figure 7. It should also be applicable to synthesize a composite containing two polyelectrolyte gels, as modeled in the present work.

Numerical results

Within a gel layer composite consisting of different materials, the occurring transport phenomena depend on the combination of the layer materials. The global material behavior can thus be altered by manipulating the properties of the individual layers. Since anionic and cationic gels show a qualitatively different transport behavior, the combination of both is of special interest, for example, for the development of target-sensitive drug carriers.

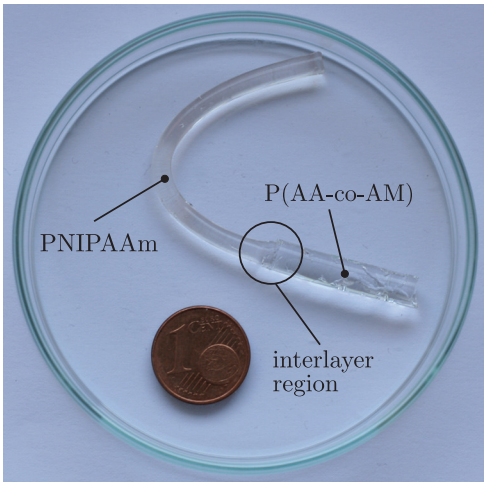

Figure 7. Hydrogel composite synthesized by combining PNIPAAm and *net*-poly(acrylamide-*co*-acrylic acid) P(AA-*co*-AM).

The modeling of the gel layer system is therefore conducted for two different test cases, (i) an anionic-anionic and (ii) an anionic-cationic hydrogel layer composite, each immersed in an ionic solution bath. A connecting interlayer between the gels is assumed and modeled as an additional thin interlayer, as discussed in the previous section. In the following, the material parameters of the interlayer $\mathcal{I}$ are treated as constant in the whole region, determined by the mean values of the respective material parameters of the neighboring gels.

Anionic-anionic gel layer system

In this section, a gel layer composed of two anionic gels $\mathcal{G}_1$ and $\mathcal{G}_2$ immersed in a solution bath $\mathcal{S}$ is investigated. The gel layer composite is chemically stimulated by a change of the ion concentration in the solution bath. In this investigation, no external electric field is imposed.

The concentration of fixed anionic groups is $c^{\mathrm{A}-} = 0.1$ mol/m^3, 0.075 mol/m^3 and 0.05 mol/m^3 for $\mathcal{G}_1$, $\mathcal{I}$ and $\mathcal{G}_2$, respectively, see Figure 9a. Fixed cationic groups are not considered in the anionic gels. The diffusion constant for the mobile ions and the relative permittivity are set to $D^{+/-} = 4.9 \times 10^{-10}$ m^2/s and $\varepsilon_r = 78$ for all domains, respectively. The investigations are conducted at a constant temperature $T = 300$ K. The velocity of the fluid is assumed to be negligible, that is, $v = 0$. Also, chemical reactions are not part of this investigation, thus the source terms are set to $r_\alpha = 0$.

To represent the aforementioned environmental conditions, boundary conditions are prescribed for the electric potential and for the mobile anion and cation concentration in the solution, at $x_{\mathrm{B1}} = 0$ and at $x_{\mathrm{B2}} = 1$ mm, see Figure 4. The chemical stimulus (change of the solution bath) is realized by a change of the prescribed ion concentration in the solution at x_{B1} and x_{B2}. It is increased from $c_0^{+/-} = 0.1$ mol/m^3 at $t = 0$ to $c^{+/-} = 0.15$ mol/m^3 for $t > 0$. For the electric potential $\Psi = 0$ at x_{B1} and at x_{B2} is prescribed for $t \geq 0$.

As initial conditions for the chemical field, concentrations of mobile anions and cations are prescribed, which are in excellent agreement with the Donnan equilibrium and the prescribed boundary conditions. The initial ion concentration for the mobile anions and cations is depicted in Figures 9c and 9d using dashed lines. The used simulation parameters are listed in Table 1.

The time integration is carried out for $0 \leq t \leq t_{\mathrm{end}} = 6000$ s with a time increment $t_{\mathrm{incr}} = 30$ s. At $t = t_{\mathrm{end}}$ the equilibrium state is defined, since the further evolution of the primary variables $c^{+/-}$ and Ψ is negligible.

Table 1. Parameters and initial ion concentrations for the simulation of the anionic-anionic gel layer composite.

		$\mathcal{S}$	$\mathcal{G}_1$	$\mathcal{I}$	$\mathcal{G}_2$
Simulation parameters	l (mm)	0.250	0.225	0.050	0.225
	N (-)	200	250	150	250
	c^{A^-} (mol/m^3)	0	0.1000	0.0750	0.0500
	c^{C^+} (mol/m^3)	0	0	0	0
	$D^{+/-}$ (m^2/s)		4.9×10^{-10}		
	ε_r (-)		78		
	T(K)		300		
Initial conditions	c^+ (mol/m^3)	0.1000	0.1618	0.1443	0.1281
	C^- (mol/m^3)	0.1000	0.0618	0.0693	0.0781
	Ψ (mV)	0	−12.440	−9.480	−6.397

Table 2. Steady state solution for the simulation of the anionic-anionic gel layer composite. The steady state is defined at t = 6000 s.

		$\mathcal{S}$	$\mathcal{G}_1$	$\mathcal{I}$	$\mathcal{G}_2$
Steady state	c^+ (mol/m^3)	0.1500	0.2081	0.1921	0.1771
	c^- (mol/m^3)	0.1500	0.1081	0.1171	0.1271
	Ψ (mV)	0	−8.4649	−6.3972	−4.2888

The spatial discretization is carried out using an adaptive mesh with an element length ratio $g = 1.2$ and with a total number of elements $n_{\text{ges}} = 1050$. The number of elements in each domain are $N = 200$, 250, 150, 250 and 200 for $\mathcal{S}$, $\mathcal{G}_1$, $\mathcal{I}$, $\mathcal{G}_2$ and $\mathcal{S}$, respectively.

The obtained results of the numerical simulation show that the ion concentration in the solution increases by $\Delta c^{+/-} = 0.05$ mol/m^3 from $t = 0$ to $t = t_{\text{end}}$ due to the change of the prescribed boundary conditions. In the gel $\mathcal{G}_1$, the interlayer $\mathcal{I}$ and the gel $\mathcal{G}_2$, an increase of the mobile anion and cation concentration of 0.0463 mol/m^3, 0.0478 mol/m^3 and 0.0490 mol/m^3 is obtained, respectively. The calculated mobile anion and cation concentrations within the different domains are depicted in Figure 9c and 9d, respectively. In both figures, the concentrations are depicted for the times $t = [0, 60, 120, 300, 6000]$ s, where the arrows indicate the development in time. In Figures 8a and 8b the anion and cation concentrations at the interface between the solution $\mathcal{S}$ and gel $\mathcal{G}_1$ at steady state are shown in detail. The obtained steady state results of the numerical simulation are listed in Table 2.

Within the gel domains, the electric potential increases with progressing time, whereas it remains almost constant within the solution domains as depicted in Figure 9b.

In close proximity to the domain interfaces a volume charge density ρ_{el} unequal to zero is found, see Figure 8c. Outside of the boundary regions electroneutrality is obtained during the whole simulation time. The volume charge density shows a "jump" ρ^{diff} at the interface between neighboring domains. This jump results from the difference of fixed charges in these domains. The obtained nonzero volume charge density at the domain interfaces yields a change in the electric potential, see Figure 9b. The resulting steady state electric potential is in excellent agreement with the analytical Donnan potential

$$\Delta\Psi = \Psi^{(s)} - \Psi^{(g)} = -\frac{1}{z_\alpha}\frac{RT}{F}\ln\left(\frac{c_\alpha^{(s)}}{c_\alpha^{(g)}}\right) \qquad (14)$$

Here the indices (s) and (g) denote two different domains (e.g. solvent and gel).

Anionic-cationic gel layer system

In this second test case, a gel layer system composed of an anionic and a cationic gel immersed in an ionic solution bath is studied. The concentration of bound anionic groups in the anionic gel $\mathcal{G}_1$ is set to $c^{A^-} = 0.09$ mol/m^3. The cationic gel $\mathcal{G}_2$ contains a concentration of bound cations $c^{C^+} = 0.11$ mol/m^3.

In analogy to the previous section, an interlayer $\mathcal{I}$ between the gels $\mathcal{G}_1$ and $\mathcal{G}_2$ is modeled. It is assumed that the interlayer contains both fixed anions and fixed cations since volume fractions of both polymer networks are present. Here, a concentration of fixed anions $c^{A^-} = 0.045$ mol/m^3 and fixed cations $c^{C^+} = 0.055$ mol/m^3 is used, see Figure 10a. The time discretization and the spatial discretization are carried out in the same manner as explained in the previous section. The parameters for the numerical simulation are listed in Table 3.

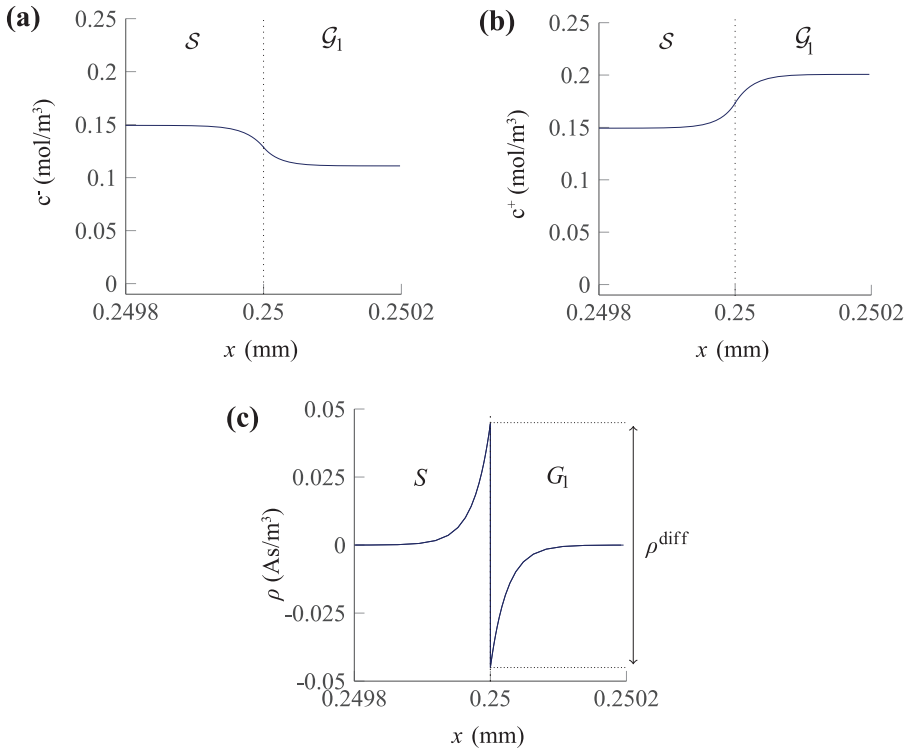

Figure 8. Steady state (a) mobile anion concentration c^-, (b) mobile cation concentration c^+ and (c) volume charge density ρ_{el} in close proximity to the interface between solution $\mathcal{S}$ and gel $\mathcal{G}_1$. Due to the change of the concentration of fixed anions between the solution and the gel layer, a jump ρ^{diff} in the value of the volume charge density is computed.

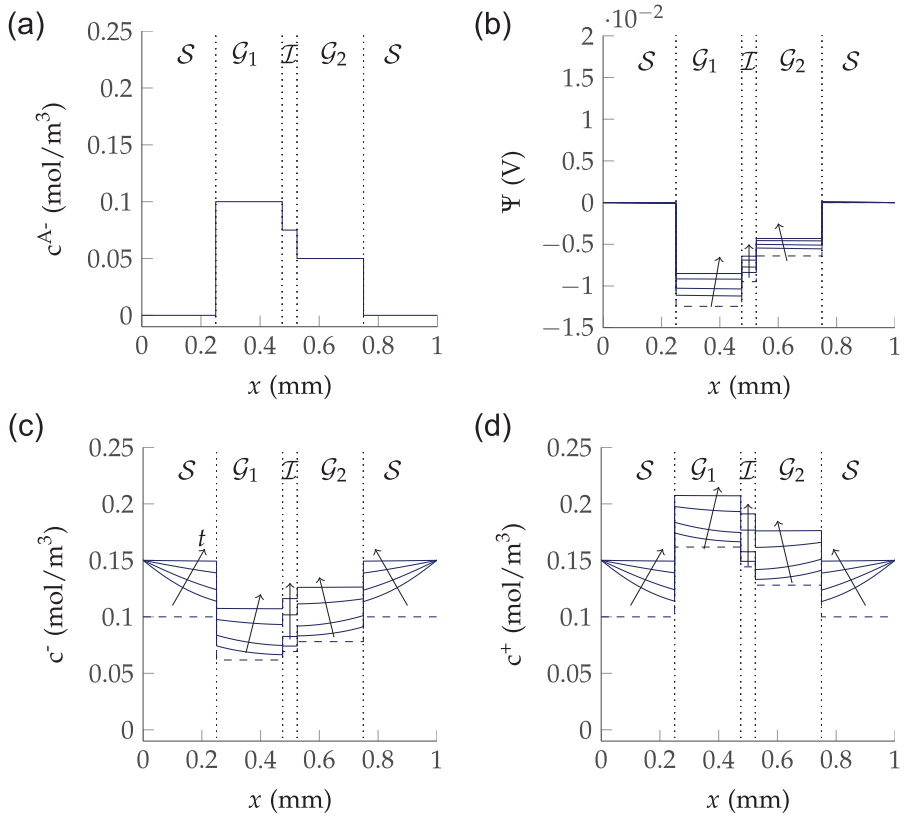

Figure 9. Results of the numerical study on the anionic-anionic gel layer composite. (a) Concentration of fixed anions, (b) electric potential, (c) concentration of mobile anions and (d) concentration of mobile cations in the layer system at t = [0, 60, 120, 300, 6000] s, where the arrows indicate the progress in time.

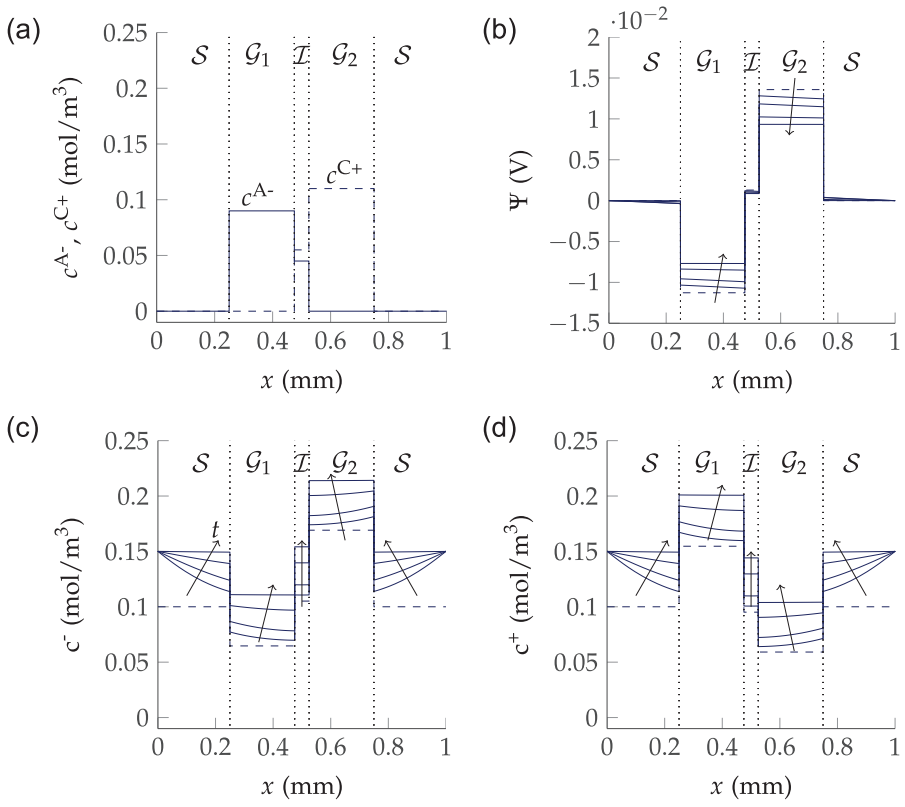

Figure 10. Results of the numerical study on the anionic-cationic gel layer composite. (a) Concentration of fixed anions (solid line) and cations (dashed line), (b) electric potential, (c) concentration of mobile anions and (d) concentration of mobile cations in the hydrogel layer system composed of an anionic and a cationic gel at t = [0, 60, 120, 300, 6000] s, where the arrows indicate the progress in time.

Table 3. Parameters and initial conditions for the simulation of the anionic-cationic gel layer composite.

		$\mathcal{S}$	$\mathcal{G}_1$	$\mathcal{I}$	$\mathcal{G}_2$
Constants	l (mm)	0.250	0.225	0.050	0.225
	N (-)	200	250	150	250
	c^{A^-} (mol/m^3)	0	0.0900	0.0450	0
	c^{C^+} (mol/m^3)	0	0	0.0550	0.1100
	$D^{+/-}$ (m^2/s)		4.9×10^{-10}		
	ε_r (-)		78		
	T (K)		300		
Initial conditions	c^+ (mol/m^3)	0.1000	0.1547	0.0951	0.0591
	c^- (mol/m^3)	0.1000	0.0647	0.1051	0.1691
	Ψ (mV)	0	−11.2721	1.2919	13.5838

With the given gel parameters, the numerical simulation is conducted in analogy to the previous section. The obtained mobile anionic and cationic concentrations are shown in Figures 10c and 10d for the times t = [0, 60, 120, 300, 6000] s, where the arrows indicate the progress in time. The concentration at initial state is depicted as a dashed line.

With progressing time, the absolute value of the electric potential within the gel domains decreases, whereas it remains almost constant within the solution. The electric potential for the times t = [0, 60, 120, 300, 6000] s is shown in Figure 10b. The obtained ion concentrations and the electric potential at steady state are listed in Table 4.

The determined electric potential difference between two neighboring domains again follows equation (14). The electric potential at steady state is negative in the domain of the anionic gel and positive in the domain of the cationic gel. Since the concentration of fixed cations is slightly higher than the concentration of fixed anions

Table 4. Steady state solution for the simulation of the anionic-cationic gel layer composite. The steady state is defined at t = 6000 s.

		$\mathcal{S}$	$\mathcal{G}_1$	$\mathcal{I}$	$\mathcal{G}_2$
Steady state	c^+ (mol/m^3)	0.1500	0.2016	0.1451	0.1048
	c^- (mol/m^3)	0.1500	0.1116	0.1551	0.2148
	Ψ (mV)	0	−7.6434	0.8615	9.2781

Table 5. Osmotic pressure at steady state within the anionic-anionic and anionic-cationic gel layer composite outside of the boundary regions.

		$\mathcal{G}_1$	$\mathcal{I}$	$\mathcal{G}_2$
Osmotic pressure difference $\Delta\pi$ (Pa)	Anionic-anionic	−18.457	−10.984	−5.437
	Anionic-cationic	−15.364	−2.793	−22.024

within the interlayer, the electric potential yields a positive value within the interlayer domain. The time to reach the equilibrium state is comparable with experimental results (Achilleos et al., 2000, 2001; De et al., 2002). In order to fabricate microfluidic devices or hydrogel based sensors, it is advantageous to achieve a faster response time. This may be realized, for example, by a reduction of the sample size or by using a more porous hydrogel. The osmotic pressure, which causes the swelling or deswelling of the polymer network can be calculated from the obtained ion distribution. The osmotic pressure for both the anionic-anionic and anionic-cationic gel layer composite will be discussed in the following section.

Evaluation of the numerical results

Using the results of the numerical simulation, the occurring osmotic pressure in the hydrogel layers can be calculated. An osmotic pressure difference $\Delta\pi$ results from the concentration differences between the different domains (Attaran et al., 2015; Wallmersperger and Ballhause, 2008). It can be described by:

$$\Delta\pi = RT \sum_{\alpha=1}^{N_f} \left[\left(\Delta c_\alpha - \Delta c_\alpha^0 \right) \right] \tag{15}$$

where $\Delta c_\alpha = c_\alpha - c_\alpha^{ref}$ and $\Delta c_\alpha^0 = c_{\alpha 0} - c_{\alpha 0}^{ref}$. Here, c_α^{ref} denotes a reference concentration of the ionic species α at the current state, $c_{\alpha 0}$ the concentration of the ionic species α at initial state and $c_{\alpha 0}^{ref}$ a reference concentration of the ionic species α at initial state.

Outside the boundary regions, the ionic concentrations at steady state are approximately constant within each domain and for each ion species. As a result, the occurring osmotic pressure also yields a constant value there. For the calculation of the osmotic pressure, the reference concentrations c_α^{ref} are defined as the concentrations of the species α in the solution $\mathcal{S}$, outside of the boundary regions, $c_{\alpha 0}^{ref}$ are the respective initial concentrations in the solution. Using these values, the osmotic pressure within the gel layers (outside of the boundary regions) can be calculated. The obtained values for the osmotic pressure at steady state are listed in Table 5. For both anionic and cationic gels, a negative value for the osmotic pressure difference is obtained.

An osmotic pressure difference causes a resulting water flux from the region of low osmotic pressure towards the region of high osmotic pressure (Cath et al., 2006). In the considered hydrogel layer system a negative osmotic pressure difference between gel and solution will, due to a resulting water release, lead to a deswelling of the hydrogel (Wallmersperger and Ballhause, 2008; Zhao, 2014). It is assumed that the deformation correlates linearly with the osmotic pressure difference and that there is no slip between adjacent gel layers. For the one-dimensional case, this will lead to a deformed state as depicted in Figure 11 (left). The gel $\mathcal{G}_1$ in the anionic-anionic gel layer composite will deswell more than the gel $\mathcal{G}_2$, as $\mathcal{G}_1$ contains more anionic groups than $\mathcal{G}_2$ and thus the relative change of the mobile ion concentration is larger. The opposite will occur in the anionic-cationic gel layer composite, as c^{C+} is larger in gel $\mathcal{G}_2$ than c^{A-} in gel $\mathcal{G}_1$.

For the two-dimensional case, a bending of the layer composite is expected. The free swelling of a hydrogel is isotropic, this means that the strain in each direction of the material is equal. Since the displacement of the gels is constrained at the boundary to the adjacent gel layer, a bending behavior will occur, see Figure 11 (right). As a result, the investigated anionic-anionic gel layer composite will bend towards gel $\mathcal{G}_1$ whereas the anionic-cationic gel layer composite will bend towards the opposite direction.

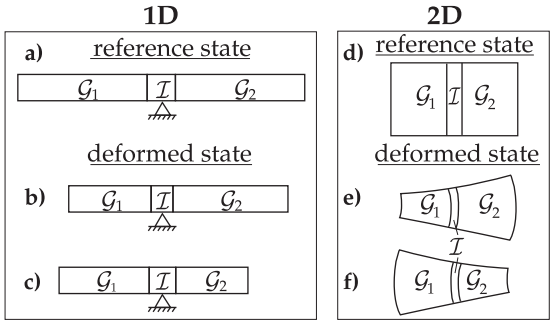

Figure 11. Schematic representation of the swelling behavior of the hydrogel layer composites in (a), (b), (c) for the 1D and in (d), (e), (f) for the 2D case. In (a) and (d) the reference states of both the anionic-anionic and the anionic-cationic hydrogel layer composites are depicted. In (b) and (e) the investigated anionic-anionic and in (c) and (f) the anionic-cationic hydrogel layer composites are shown in the deformed state. The derived change in length from the 1D case results in a bending behavior in the 2D case. The bending occurs towards the gel layer with the higher fixed ion concentration.

Conclusion and outlook

Hydrogel layer composites exhibit desirable properties for novel applications such as microfluidic devices and target-selective drug carriers. The effects occurring within the layer systems are rather complex and their behavior is challenging to model. Since only few research groups numerically investigated these composites, a gap remained to specifically describe the transient ion distribution and the electric field within the gel layers systems. The present article filled this gap by numerically investigating the electro-chemical behavior of anionic-anionic and anionic-cationic gel layer composites, as both combinations are relevant for possible applications.

A multifield theory was adopted to model this behavior. To solve the nonlinear field problem, the finite element method was applied. Suitable boundary, transition and initial conditions to represent an external chemical stimulus were given. The simulation results for the transient ion distribution and the electric potential were presented and discussed. Based on the obtained results the steady-state osmotic pressure was obtained and the bending behavior predicted. The magnitude of this bending is dependent on the concentration difference of fixed charged groups between the layers.

The numerical solution of the system of partial differential equations is in excellent agreement with the analytical solution. Therefore, the applied method is predestined for modeling hydrogel layer systems for microfluidic devices and drug delivery systems.

Acknowledgement

The authors want to thank Andreas Krause from the Leibniz Institute for Polymer Research Dresden for preparing the hydrogel-layer composite P(AA-*co*-AM).

Declaration of Conflicting Interests

The author(s) declared no potential conflicts of interest with respect to the research, authorship, and/or publication of this article.

Funding

The author(s) disclosed receipt of the following financial support for the research, authorship, and/or publication of this article: This work was supported by the German Research Foundation (DFG) in the framework of the research training group GRK "Hydrogel-based microsystems" (DFG-GRK 1865).

References

Acartürk A, Ehlers W, Abbas I, et al. (2003) A 3-D model for finite viscoelsatic swelling of charged tissues and gels. *Proceedings in Applied Mathematics and Mechanics* 3(1): 242–243.

Achilleos EV, Christodoulou KN and Kevrekidis IG (2000) A transport model for swelling of polyelectrolyte gels in simple and complex geometries. *American Institute of Chemical Engineers* 46(11): 2128–2139.

Achilleos EV, Prud'homme RK, Kevrekidis IG, et al. (2001) A 3-D model for finite viscoelastic swelling of charged tissues and gels. *Computational and Theoretical Polymer Science* 11(1): 63–80.

Arndt MC and Sadowski G (2013) Thermodynamic modelling of hydrogel systems. In: *Intelligent Hydrogels*. London: Springer, pp.175–187.

Attaran A, Brummund J and Wallmersperger T (2015) Modeling and simulation of the bending behavior of electrically-stimulated cantilevered hydrogels. *Smart Materials and Structures* 24(3): 035021.

Ballhause D and Wallmersperger T (2008) Coupled chemo-electro-mechanical finite element simulation of hydrogels: I. chemical stimulation. *Smart Materials and Structures* 17(4): 045011.

Bowen RM (1980) Incompressible porous media models by use of the theory of mixtures. *International Journal of Engineering Science* 18(9): 1129–1148.

Brock D, Lee W, Segalman D, et al. (1994) A dynamic model of a linear actuator based on polymer hydrogel. *Journal of Intelligent Material Systems and Structures* 5(6): 764–771.

Cath TY, Lee W, Childress AE, et al. (2006) Forward osmosis: Principles, applications, and recent developments. *Journal of Membrane Science* 281(1–2): 70–87.

De S, Aluru N, Johnson B, et al. (2002) Equilibrium swelling and kinetics of ph-responsive hydrogels: Models, experiments, and simulations. *Journal of Microelectromechanical Systems* 11(5): 544–555.

de Gennes PG, Okumura K, Shahinpoor M, et al. (2000) Mechanoelectric effects in ionic gels. *Europhysics Letters* 50(4): 513.

Doi M, Matsumoto M and Hirose Y (1992) Deformation of ionic polymer gels by electric fields. *Macromolecules* 25(20): 5504–5511.

Ehlers W, Acartürk A and Markert B (2003a) A continuum approach for the swelling of charged hydrated media. In: *Analysis and Simulation of Multifield Problems*. Berlin: Springer, pp.271–277.

Ehlers W, Acartürk A and Markert B (2003b) Modelling of 3-D linear viscoelastic swelling of charged tissues and gels. *Proceedings in Applied Mathematics and Mechanics* 2(1): 218–219.

Ermatchkov V, Ninni L and Maurer G (2010) Thermodynamics of phase equilibrium for systems containing n-isopropyl acrylamide hydrogels. *Fluid Phase Equilibria* 296(2): 140–148.

Farinholt K and Leo D (2004) Modeling of electromechanical charge sensing in ionic polymer transducers. *Mechanics of Materials* 36(5–6): 421–433.

Flory PJ and Rehner J (1943a) Statistical mechanics of cross-linked polymer networks i. rubberlike elasticity. *The Journal of Chemical Physics* 11(11): 512–520.

Flory PJ and Rehner J (1943b) Statistical mechanics of cross-linked polymer networks ii. swelling. *The Journal of Chemical Physics* 11(11): 521–526.

Fulghum TM, Estillore NC, Vo CD, et al. (2008) Stimuli-responsive polymer ultrathin films with a binary architecture: Combined layer-by-layer polyelectrolyte and surface-initiated polymerization approach. *Macromolecules* 41(2): 429–435.

Gerlach G, Guenther M, Sorber J, et al. (2005) Chemical and pH sensors based on the swelling behavior of hydrogels. *Sensors and Actuators B: Chemical* 111: 555–561.

Grimshaw PE, Nussbaum JH, Grodzinsky AJ, et al. (1990) Kinetics of electrically and chemically induced swelling in polyelectrolyte gels. *The Journal of Chemical Physics* 93(6): 4462–4472.

Guenther M, Gerlach G and Wallmersperger T (2009) Nonlinear effects in hydrogel-based chemical sensors: Experiment and modeling. *Journal of Intelligent Material Systems and Structures* 93(6): 4462–4472.

Harmon ME, Jakob TAM, Knoll W, et al. (2002) A surface plasmon resonance study of volume phase transitions in n-isopropylacrylamide gel films. *Macromolecules* 35(15): 5999–6004.

Hiller J and Rubner MF (2003) Reversible molecular memory and pH-switchable swelling transitions in polyelectrolyte multilayers. *Macromolecules* 36(11): 4078–4083.

Huyghe J and Janssen J (1997) Quadriphasic mechanics of swelling incompressible porous media. *International Journal of Engineering Science* 35(8): 793–802.

Jaber JA and Schlenoff JB (2005) Polyelectrolyte multilayers with reversible thermal responsivity. *Macromolecules* 38(4): 1300–1306.

Jeong B and Gutowska A (2002) Lessons from nature: Stimuli-responsive polymers and their biomedical applications. *Trends in Biotechnology* 20(7): 305–311.

Johnson T and Amirouche F (2008) Multiphysics modeling of an IPMC microfluidic control device. *Microsystem Technologies* 14(6): 871–879.

Keller K, Wallmersperger T, Kröplin B, et al. (2011) Modeling of temperature-sensitive polyelectrolyte gels by the use of the coupled chemo-electro-mechanical formulation. *Mechanics of Advanced Materials and Structures* 18(7): 511–523.

Kharlampieva E, Kozlovskaya V, Tyutina J, et al. (2005) Hydrogen-bonded multilayers of thermoresponsive polymers. *Macromolecules* 38(25): 10523–10531.

Kuckling D, Harmon ME and Frank CW (2002) Photo-crosslinkable PNIPAAm copolymers. 1. synthesis and characterization of constrained temperature-responsive hydrogel layers. *Macromolecules* 35(16): 6377–6383.

Lai W, Hou J and Mow V (1991) A triphasic theory for the swelling and deformation behaviors of articular cartilage. *Journal of Biomechanical Engineering* 113(3): 245–258.

Li H, Luo R and Lam K (2007) Modeling of ionic transport in electric-stimulus-responsive hydrogels. *Journal of Membrane Science* 289(1–2): 284–296.

Li H, Ng T, Cheng J, et al. (2003) Hermite-cloud: A novel true meshless method. *Computational Mechanics* 33(1): 30–41.

Lu S, Ramirez WF and Anseth KS (1998) Modeling and optimization of drug release from laminated polymer matrix devices. *American Institute of Chemical Engineers* 44(7): 1689–1696.

Lu S, Ramirez WF and Anseth KS (2000) Photopolymerized, multilaminated matrix devices with optimized nonuniform initial concentration profiles to control drug release. *Journal of Pharmaceutical Sciences* 89(1): 45–51.

Lucantonio A, Nardinocchi P and Pezzulla M (2014) Swelling-induced and controlled curving in layered gel beams. *Proceedings of the Royal Society A: Mathematical, Physical and Engineering Science* 470(2171): 20140467.

Mann BA, Holm C and Kremer K (2005) Swelling of polyelectrolyte networks. *The Journal of Chemical Physics* 122(15): 154903.

Mann BA, Kremer K and Holm C (2005) The swelling behavior of charged hydrogels. *Macromolecular Symposia* 237(1): 90–107.

Nolan CM, Serpe MJ and Lyon LA (2004) Thermally modulated insulin release from microgel thin films. *Biomacromolecules* 5(5): 1940–1946.

Nykänen A, Nuopponen M, Laukkanen A, et al. (2007) Phase behavior and temperature-responsive molecular filters based on self-assembly of polystyrene-block-poly(n-isopropylacrylamide)-block-polystyrene. *Macromolecules* 40(16): 5827–5834.

Orlov Y, Xu X and Maurer G (2006) Equilibrium swelling of n-isopropyl acrylamide based ionic hydrogels in aqueous solutions of organic solvents: Comparison of experiment with theory. *Fluid Phase Equilibria* 249(1–2): 6–16.

Orlov Y, Xu X and Maurer G (2007) An experimental and theoretical investigation on the swelling of n-isopropyl acrylamide based ionic hydrogels in aqueous solutions of (sodium chloride or di-sodium hydrogen phosphate). *Fluid Phase Equilibria* 254(1–2): 1–106.

Osada Y and Gong JP (1998) Advanced Materials. *Fluid Phase Equilibria* 10(11): 827–837.

Prudnikova K and Utz M (2012) Electromechanical equilibrium properties of poly(acrylic acid/acrylamide) hydrogels. *Macromolecules* 45(2): 1041–1045.

Qiu Y and Park K (2001) Environment-sensitive hydrogels for drug delivery. *Advanced Drug Delivery Reviews* 53(3): 321–339.

Richter A, Bund A, Keller M, et al. (2004) Characterization of a microgravimetric sensor based on pH sensitive hydrogels. *Sensors and Actuators B: Chemical* 99(2–3): 579–585.

Serpe MJ, Yarmey KA, Nolan CM, et al. (2005) Doxorubicin uptake and release from microgel thin films. *Biomacromolecules* 6(1): 408–413.

Shahinpoor M (1995) Micro-electro-mechanics of ionic polymeric gels as electrically controllable artificial muscles. *Journal of Intelligent Material Systems and Structures* 6(3): 307–314.

Shiga T and Kurauchi T (1990) Deformation of polyelectrolyte gels under the influence of electric field. *Journal of Applied Polymer Science* 39(11–12): 2305–2320.

Slomkowski S, Alemán JV, Gilbert RG, et al. (2011) Terminology of polymers and polymerization processes in dispersed systems (IUPAC recommendations 2011). *Pure and Applied Chemistry* 83: 2229–2259.

Sohier J, Vlugt T, Cabrol N, et al. (2006) Dual release of proteins from porous polymeric scaffolds. *Journal of Controlled Release* 111(1–2): 95–106.

Sun D, Gu W, Guo X, et al. (1999) A mixed finite element formulation of triphasic mechano-electrochemical theory for charged, hydrated biological soft tissues. *International Journal for Numerical Methods in Engineering* 45(10): 1375–1402.

Tokarev I and Minko S (2009) Stimuli-responsive hydrogel thin films. *Soft Matter* 5: 511–524.

van Loon R, Huyghe JM, Wijlaars MW, et al. (2003) 3D FE implementation of an incompressible quadriphasic mixture model. *International Journal for Numerical Methods in Engineering* 57(9): 1243–1258.

Wallmersperger T, Kröplin B and Gülch RW (2001) Coupled multifield formulation for ionic polymer gels in electric fields. *Proceedings of SPIE, Smart Structures and Materials* 4329: 264–275.

Wallmersperger T and Ballhause D (2008) Coupled chemo-electro-mechanical finite element simulation of hydrogels: Ii. electrical stimulation. *Smart Materials and Structures* 17(4): 045012.

Wallmersperger T, Kröplin B and Gülch RW (2004) Coupled chemo-electro-mechanical formulation for ionic polymer gels - numerical and experimental investigations. *Mechanics of Materials* 36(5–6): 411–420.

Walter J, Ermatchkov V, Vrabec J, et al. (2010) Molecular dynamics and experimental study of conformation change of poly (n-isopropylacrylamide) hydrogels in water. *Fluid Phase Equilibria* 296(2): 164–172.

Wu S, Li H, Chen JP, et al. (2004) Modeling investigation of hydrogel volume transition. *Macromolecular Theory and Simulations* 13: 13–29.

Zhao S (2014) Osmotic pressure versus swelling pressure: Comment on "Bifunctional polymer hydrogel layers as forward osmosis draw agents for continuous production of fresh water using solar energy". *Environmental Science & Technology* 48(7): 4212–4213.